ELSEVIER

Chemical Engineering Journal 121 (2006) 65–71

Chemical Engineering Journal

www.elsevier.com/locate/cej

Mechanochemical effects on the molybdenite roasting kinetics

Reza Ebrahimi-Kahrizsangi *, Mohammad Hasan Abbasi, Ali Saidi

Department of Materials Engineering, Isfahan University of Technology, Isfahan, Iran

Received 2 December 2005; received in revised form 22 April 2006; accepted 26 April 2006

Abstract

The kinetics of molybdenite roasting was studied by non-isothermal TGA–DTA with heating rate 10 °C min^{-1}. Mechanical activation of molybdenite was accomplished via milling in a planetary mill under air atmosphere. Mechanical activation decreased the ignition temperature of reaction from 470 to 180 °C after 36 h of milling. The model-fitting kinetic approach has been applied to TGA data. The reaction mechanism for non-activated molybdenite was determined to be chemically controlled with $E = 34.25$ kcal mol^{-1} and $A = 2 \times 10^8$ s^{-1}. In the activated molybdenite the reaction mechanism changed to diffusion control with $E = 60.55$ kcal mol^{-1} and $A = 6 \times 10^{19}$ s^{-1}.

Keywords: Molybdenite; Mechanical activation; Kinetics; Non-isothermal; Oxidation; TGA–DTA

1. Introduction

1.1. Mechanical activation

Mechanical activation of solid substances is one of the components of modern scientific disciplines of mechanochemistry. At present, mechanochemistry appears to be a science with a sound theoretical foundation which exhibits a wide range of potential application [1]. The process involves prolonged milling to produce finely ground particles with increase in lattice strain and lattice defects that increase the molar Gibbs free energy of milled particles and exhibit enhanced reaction rates [2].

The literature on the subject is quite extensive and several review articles have appeared summarizing the earlier studies. Fox [3] has given historical overview of this subject. In another review Lin and Nadiv [4] discussed the mechonochemical phenomena in polymorphic phase transformation and synthesis of inorganic solids and alloys. Butyagin [5] has given a brief review in the foundation of mechanochemistry as an independent branch of chemical science.

In the field of extractive metallurgy many works have been carried out on the sulfidic concentrates [1]. Hu et al. [6] investigated the effect of mechanical activation of molybdenite by studying the structural changes of non-activated and mechanically activated molybdenite. In this study the effect of mechanical activation on the temperature and kinetics of molybdenite oxidation was studied.

1.2. Molybdenite oxidation

The starting material for all pyro-processes of Molybdenum is the molybdenite concentrate. Almost all molybdenite concentrate are first Subjected to roasting to yield technical grade molybdic oxide which forms the basic raw material for all commercially used products of molybdenum. The roasting of molybdenite concentrate involves a number of chemical reactions [7]. In the main reaction molybdenite reacts rapidly and exothermically with oxygen and yields molybdenum trioxide

$$MoS_2 + 3.5O_2 \rightarrow MoO_3 + 2SO_2 \quad (1)$$

The change in the standard free energy of the oxidized roasting of molybdenite is given by the following equation [8]

$$\Delta G^0\,(\text{cal mol}^{-1}) = -256870 + 14.67T \log T - 5.4 \times 10^{-3}T^2 + 0.62 \times 10^{-6}T^3 + 13.8T$$

Equilibrium constant of the reaction at 400 and 600 °C are 1.18×10^{72} and 6.21×10^{52}, respectively. It is observed that the equilibrium constant is very large and the reaction of the oxidized roasting of molybdenite is considered in practice to be an irreversible one and takes place even at very low concentration of oxygen. There is another reaction that leads to the formation

* Corresponding author. Tel.: +98 3113912750; fax: +98 3113912751.
E-mail address: rezaebrahimi@iaun.ac.ir (R. Ebrahimi-Kahrizsangi).

1385-8947/$ – see front matter © 2006 Elsevier B.V. All rights reserved.
doi:10.1016/j.cej.2006.04.011

Nomenclature

A	pre-exponential factor (s^{-1})
E_a	activation energy (kcal mol^{-1})
$f(\alpha)$	differential reaction model
$g(\alpha)$	integral reaction model
$k(T)$	rate constant (s^{-1})
$p(x)$	exponential integral
r	radius of particle (cm)
R	gas constant (1.987 cal mol^{-1} K^{-1})
T	temperature
$\bar{T}$	mean experimental temperature
t	time (s)

Greek letters

α	extent of reaction
β	heating rate (K min^{-1})

of molybdenum dioxide

$$MoS_2 + 3O_2 \rightarrow MoO_2 + 2SO_2 \quad (2)$$

Since molybdenum dioxide is practically insoluble in ammonia water, in order to decrease the MoO_2 fraction and avoid sintering it is necessary to carry out roasting at low temperature. The mechanical activation of minerals makes it possible to reduce their decomposition temperature or causes such a degree of disordering that the thermal activation may be omitted entirely. In this process the complex influence of surface and bulk properties occur. The mineral activation leads to a positive influence on the reaction kinetics. At present it is not known whether the kinetics of heterogeneous reaction is determined by the contact area, the structure of mineral or both. The required modification of the structure can be achieved by mechanical activation of the mineral, typically by intensive grinding. The breaking of bonds in the crystalline lattice of the mineral brings about a decrease in activation energy and an increase in the rate of reaction.

1.3. Rate law and kinetics analysis

The kinetics of molybdenite oxidation can be studied by thermogravimetry method. In most of the reported TGA studies the temperature of sample was linearly increased.

The rate of a solid state reaction can be generally described by

$$\frac{d\alpha}{dt} = k(T) f(\alpha) \quad (3)$$

Integration of the above equation gives the integral rate law

$$g(\alpha) = kt \quad (4)$$

Several reaction models [9] using $f(\alpha)$ or $g(\alpha)$ are listed in Table 1. The explicit temperature dependence of the rate constant is introduced by replacing $k(T)$ with the Arrhenius equation which gives

$$\frac{d\alpha}{dt} = A \exp\left(\frac{-E_a}{RT}\right) f(\alpha) \quad (5)$$

And

$$g(\alpha) = A \exp\left(\frac{-E_a}{RT}\right) t \quad (6)$$

where A (the pre-exponential factor) and E (activation energy) are the Arrhenius parameters. The Arrhenius parameters together with the reaction model are sometimes called the kinetics triplet. Under non-isothermal conditions in which a sample heated at a constant rate, the explicit temporal in Eq. (5) is eliminated through the trivial transformation

$$\frac{d\alpha}{dT} = \frac{A}{\beta} \exp\left(\frac{-E_a}{RT}\right) f(\alpha) \quad (7)$$

Upon integration Eq. (7) gives

$$g(\alpha) = \frac{A}{\beta} \int_0^T e^{(-E_a/RT)}\, dT \quad (8)$$

If E_a/RT is replaced by x and integration limits transformed Eq. (8) becomes,

$$g(\alpha) = \frac{AE_a}{RT} \int_x^\infty \frac{e^{-x}}{x^2}\, dx \quad (9)$$

Eq. (9) can be written as

$$g(\alpha) = \frac{AE_a}{RT} p(x) \quad (10)$$

The $p(x)$ has no analytical solution but has many approximations [10]. Kinetics parameters can be obtained from non-isothermal rate laws by both model-fitting and isoconversional (model-free) methods [11,12]. Model-fitting methods involve fitting different models to α-temperature curves and simultaneously determining the activation energy (E) and frequency factor (A). There are several non-isothermal model-fitting methods. One of the most popular being the Coats and Redfern method [13]. This method utilizes the asymptotic series expansion for approximating the exponential integral in Eq. (10) giving

$$\ln \frac{g(\alpha)}{T^2} = \ln\left[\frac{AR}{\beta E_a}\left(1 - \frac{2R\bar{T}}{E_a}\right)\right] - \frac{E_a}{RT} \quad (11)$$

Plotting the left hand side of Eq. (11), which includes the model $g(\alpha)$ versus $1/T$ gives E_a and A from the slope and intercept, respectively. The model that gives the best linear fit is selected as the chosen model.

2. Experimental

This research was carried out with molybdenite samples from the Sarcheshmeh Copper industries in Iran with 0.99 m^2 g^{-1} specific surface area and particle size in the range of 60–80 μm. The chemical composition of the studied molybdenite is Mo: 55.9%, Cu: 1.1%, S: 39%

Mechanical activation was accomplished via milling in a FP2 planetary mill under air atmosphere using a 20:1 charge ratio

Table 1
Solid state reaction rate models

Reaction model	$f(\alpha)$	$g(\alpha)$
Nucleation models		
1. Power law	$4\alpha^{3/4}$	$\alpha^{1/4}$
2. Power law	$3\alpha^{2/3}$	$\alpha^{1/3}$
3. Power law	$2\alpha^{1/2}$	$\alpha^{1/2}$
4. Avrami–Erofeev	$4(1-\alpha)[-\ln(1-\alpha)]^{3/4}$	$[-\ln(1-\alpha)]^{1/4}$
5. Avrami–Erofeev	$3(1-\alpha)[-\ln(1-\alpha)]^{2/3}$	$[-\ln(1-\alpha)]^{1/3}$
6. Avrami–Erofeev	$2(1-\alpha)[-\ln(1-\alpha)]^{1/2}$	$[-\ln(1-\alpha)]^{1/2}$
Diffusion models		
7. One-dimensional diffusion	$(1/2)\alpha^{-1}$	α^2
8. Diffusion control (janders)	$2(1-\alpha)^{2/3}[1-(1-\alpha)^{1/3}]-1$	$[1-(1-\alpha)^{1/3}]^2$
9. Diffusion control (crank)	$(3/2)[(1-\alpha)^{-1/3}-1]^{-1}$	$1-(2/3)\alpha-(1-\alpha)^{2/3}$
Reaction order and geometrical contraction models		
10. Mampel (first order)	$1-\alpha$	$-\ln(1-\alpha)$
11. Second order	$(1-\alpha)^2$	$(1-\alpha)^{-1}-1$
12. Contracting cylinder	$2(1-\alpha)^{1/2}$	$1-(1-\alpha)^{1/2}$
13. Contracting sphere	$3(1-\alpha)^{2/3}$	$1-(1-\alpha)^{1/3}$

(the mass of grinding media to mass of concentrate) and a filling factor of 0.3 (volume of charge/volume of mill). The milling media used was stainless steel vial and balls of 20 mm diameter. The grinding times up to 36 h examined. The specific surface area was measured by BET method by using a Micromeritics Gemini instrument.

A Mettler Tuledu Star System was used for simultaneous TGA–DTA studies. Experiments were performed under non-isothermal condition at programmed linear heating rate of 10 °C min^{-1}. The initial weight of samples was 36 mg. Oxygen flowing was used for molybdenite oxidation and flow rate was maintained at 50 ml min^{-1}.

The starting material and products were analyzed by employing Philips X-pert X-ray diffractometer with PW 2273 tube and Cu Kα radiation with scan rate 0.04° s^{-1}. A LEO scanning electron microscope was used to study the shape and size of particles.

3. Results and discussion

Fig. 1 shows XRD patterns of unmilled (as received) and activated concentrate in different times. Mechanical activation causes the decrease in intensity of diffraction lines, the shift in diffraction lines and the diffraction line broadening. The decrease in intensity of diffraction lines is the result of decrease in crystalline phase. The shift in diffraction lines is due to uniform strain. The X-ray diffraction line profile obtained in a diffractometer is broadened due to instrumental and physical (crystallite size and lattice strain) factors. The intensity of (0 0 l) (l = 2, 6, 8, 10) planes show more change with mechanical activation. This indicated that the flaky structure of molybdenite distorted during mechanical activation.

The effect of milling time on the specific surface of molybdenite is represented in Fig. 2. In this case the specific adsorption surface reaches the maximum at 5 h milling and afterwards its value decreases to a constant value. This decrease is due to formation of Agglomerates. Similar trend of the specific adsorption surface was reported for chalcopyrite [14].

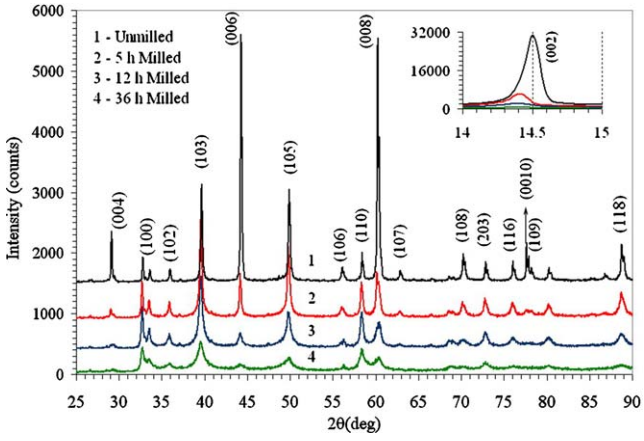

Fig. 1. XRD patterns of unmilled (as received) and activated concentrate in different times.

Figs. 3 and 4 show TGA and DTA curves for oxidation of molybdenite concentrate unmilled and milled at different times.

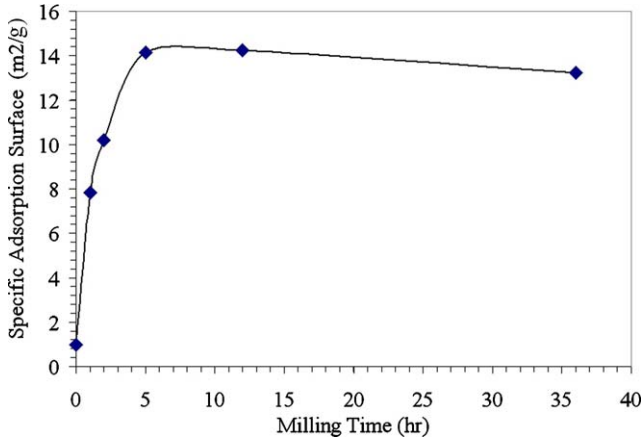

Fig. 2. Specific adsorption surface of molybdenite concentrate vs. milling time.

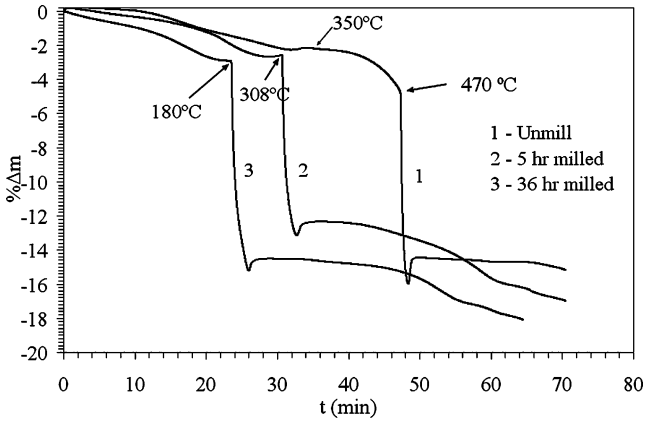

Fig. 3. TGA curves for non-isothermal oxidation of molybdenite concentrate unmilled and milled at different times.

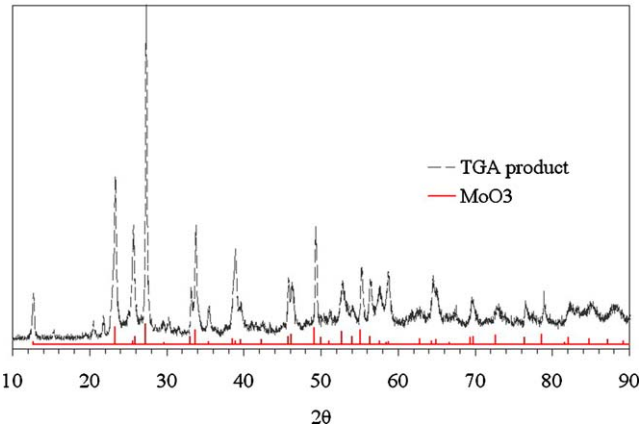

Fig. 5. XRD pattern of TGA product at the end stage of mass decreasing.

As seen from these curves the oxidation of molybdenite is characterized by exothermic peak in the DTA curves. Mechanical activation shifts the peak temperature at 470 to 308 °C and 180 °C after 5 and 36 h milling, respectively. The corresponding TGA curves in Fig. 3 also show a shift in onset temperature of the process accompanied by a high mass decrease. The TGA curves show a mass increase at the end stage of oxidation. This increase is due to oxidation of MoO_2 to MoO_3. So we have some MoO_2 formation during molybdenite oxidation. According to stoichiometric reactions the percent of mass decrease for complete oxidation of MoS_2 to MoO_3 and/or MoO_2 is 10% and 20%, respectively. If we consider the mass of sample at ignition temperature as w_0, the percent of mass decrease in different samples will be 11–12%. This indicates that most of MoS_2 has been oxidized to MoO_3. Fig. 5 shows the XRD pattern of TGA product at the end stage of mass decreasing and represent that almost all product is MoO_3.

Using the TGA data the extent of reaction was calculated by the following equation

$$\alpha = \frac{w_0 - w_t}{Bw_0} \tag{12}$$

where w_0 and w_t are the masses of the sample initially and at time t, respectively, and B is the fraction of weight loss for complete oxidation of MoS_2. In this study the weight of TGA sample at 470 °C (for unmilled sample) and at 308 and 180 °C (for milled samples) is considered as w_0. Fig. 6 illustrates the variation of α versus time after ignition of reaction for milled and unmilled samples.

It seems that milling of sample for 5 h changed the mechanism and reaction rate but prolongation of milling time after 5 h has not reasonable effect on the kinetics of oxidation. Also prolongation of milling time decreases the ignition temperature of reaction.

By inserting various $g(\alpha)$ into Eq. (11) Arrhenius parameters were determined from the plot $\ln g(\alpha)/T^2$ against T^{-1}.

The set of Arrhenius parameters for molybdenite oxidation in the unmilled and 5 h milled samples are shown in Table 2.

From the view point of pre-exponential factors for the solid state reactions the theoretical values are 10^6–10^{18} s^{-1}, [15].

In Table 2 all nucleation models (1–6) have very small pre-exponential factors indicating that these models cannot explain the reaction mechanism.

For the remaining models the goodness of fit is customarily estimated by a coefficient of linear correlation, r. A single

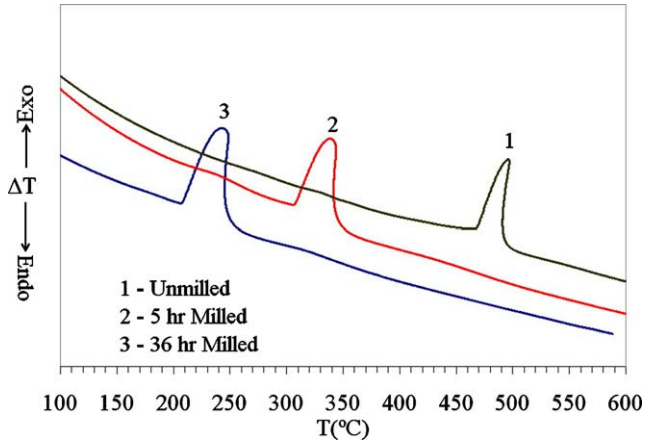

Fig. 4. DTA curves for non-isothermal oxidation of molybdenite concentrate unmilled and milled at different times.

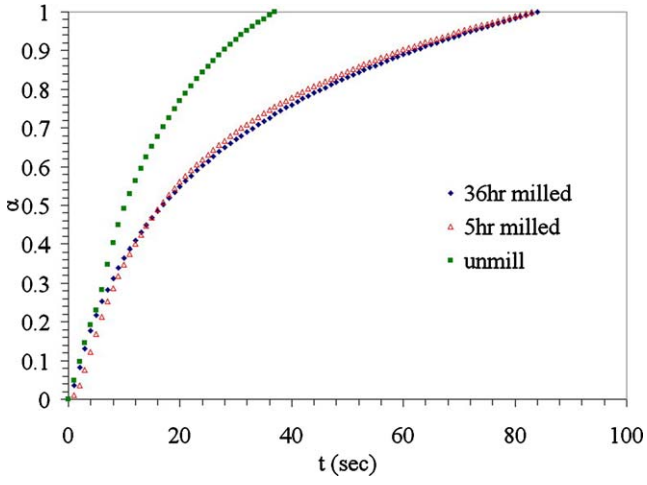

Fig. 6. Variation of extent of oxidation vs. time after ignition of reaction for milled and unmilled samples.

Table 2
Arrhenius parameters for non-isothermal oxidation of molybdenite for unmilled and 5 h milled samples

Model	Unmilled sample			5 h milled sample		
	E (kcal mol^{-1})	A (s^{-1})	$-r$	E (kcal mol^{-1})	A (s^{-1})	$-r$
1	8	4.25	0.9235	3.34	0.0411	0.8768
2	9.2	17.5	0.9145	5.1	1.08	0.9194
3	15.7	1.75	0.9015	9.08	4.88	0.9271
4	6.48	2.81	0.9264	11.5	141	0.9321
5	9.56	23.73	0.9084	14.07	583	0.9605
6	15.73	1.68×10^{3}	0.9321	22.23	8.9×10^{5}	0.9916
7	70.3	3.05×10^{18}	0.9421	43.49	3.62×10^{13}	0.9480
8	74	4×10^{19}	0.9361	60.55	6×10^{19}	0.9862
9	70	5.6×10^{17}	0.9325	61.52	3.49×10^{19}	0.9761
10	37	4.1×10^{12}	0.9994	46.97	2.03×10^{15}	0.9925
11	35.39	1.03×10^{9}	0.9993	93.9	1.03×10^{22}	0.9124
12	35.7	4×10^{8}	0.9993	31.33	9.68×10^{8}	0.9783
13	34.25	2×10^{8}	0.9994	35.96	3.98×10^{10}	0.9853

pair of E and A is then commonly chosen as that corresponding to a reaction model that gives rise to the maximum absolute value of the correlation coefficient, $|r_{max}|$ [16–19]. As seen from Table 2 all reaction models for oxidation of unmilled and milled molybdenite have correlation coefficient greater than 0.9. This popular routine ignores the fact that the correlation coefficient is subject to random fluctuations, and its uncertainty must be taken into account in the form of confidence limits. Within these limits, all models are equally probable. Thus, we use the Arrhenius parameters listed in Table 2 to predict variation of α versus time using models 7–13 in non-isothermal condition and compare these data with experimental data. Fig. 7 shows prediction of non-isothermal oxidation kinetics of unmilled molybdenite with experimental data obtained from TGA curve. The resulting values of α in Fig. 6 and experimental α allows the contracting sphere model (number 13) to be identified as the best description for non-isothermal oxidation of molybdenite for reaction extent less than 0.6. The corresponding Arrhenius parameters are $E = 34.25$ kcal mol^{-1} and $A = 2 \times 10^{8}$ s^{-1}. This value is equal to Abdel-Rehim work [10] in the isothermal oxidation of molybdenite at 450 °C.

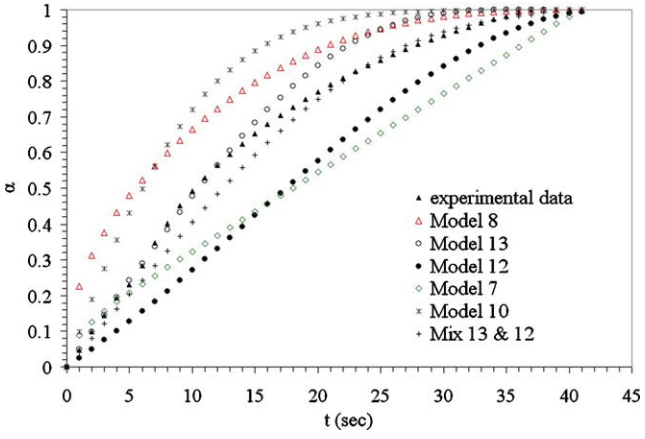

Fig. 7. Modeling of non-isothermal oxidation kinetics of unmilled molybdenite with experimental data obtained from TGA curve.

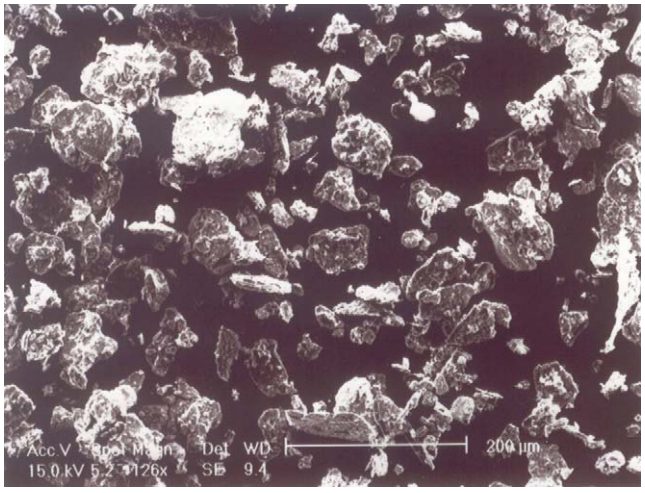

Fig. 8. SEM micrograph of unmilled molybdenite concentrate at 480 °C.

For α greater than 0.6 a mixed control mechanism of models 12 and 13 has the best fit with experimental data. Both of these models are chemically controlled mechanism for two different shapes of particles. Figs. 8 and 9 show micrograph

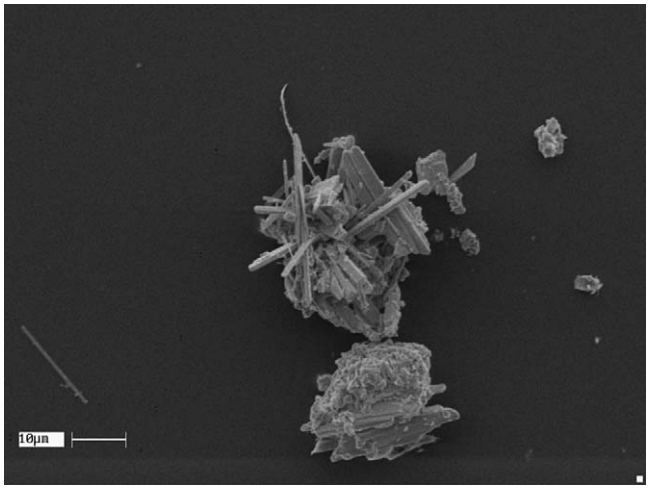

Fig. 9. SEM micrograph of TGA product at 480 °C.

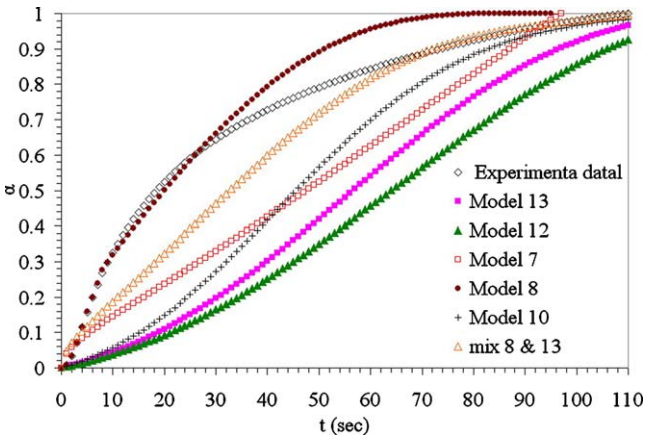

Fig. 10. Modeling of non-isothermal oxidation kinetics of 5 h milled molybdenite with experimental data obtained from TGA curve.

of unmilled molybdenite concentrate and TGA product at 480 °C, respectively. As seen from these micrographs, by increasing in the temperature molybdic oxide crystallizes to polyhedral and acicular shapes that growth directionally. This phenomenon changes the particles shape. Directional crystallization of MoO_3 could remove oxide layer from the surface of MoS_2 particles, thus by increasing in the reaction extent the mechanism of oxidation do not change to diffusion control.

Fig. 10 shows modeling of non-isothermal oxidation kinetics of 5 h milled molybdenite with experimental data obtained from TGA curve. The resulting values of α in Fig. 10 and experimental α allows the diffusion control model (number 8) to be identified as the best description for non-isothermal oxidation of activated molybdenite for the reaction extent less than 0.6. The corresponding Arrhenius parameters are $E = 60.55\,\text{kcal mol}^{-1}$ and $A = 6 \times 10^{19}\,\text{s}^{-1}$. The reason for the existence of this mechanism at the beginning stage of oxidation is that during milling of molybdenite concentrate a thin and condensed film of molybdenum oxide forms on the surface of molybdenite particles. Thus in the next oxidation process oxygen must diffuse through this oxide layer and react with MoS_2. Increasing the reaction extent and temperature, and directional crystallization of MoO_3 causes porosity and cracks formation in the particles. Thus a dense oxide layer will be changed to a porous layer and this affects the reaction mechanism. Fig. 11 shows crystallization and delaminating of oxide layer and formation of porosity in TGA product of 36 h milled molybdenite. In activated samples for extent of reaction greater than 0.6 the reaction mechanism changed. It seems that at the reaction extent greater than 0.7 a mixed mechanism of diffusion (model 8) and chemical control (model 13) has the best fit with experimental data. It can be seen that in the activated samples both the activation energy and pre-exponential factor increased and the reaction rate is faster than unmilled sample. The reason for the increase in the reaction rate is that in the heterogeneous reactions, when the reaction is chemically controlled, the rate is proportional to r^{-1} and when the reaction mechanism is diffusion control the rate is proportional to r^{-2}. The primary effect of mechanical activation is comminution of particles which reduces the r and increases the reaction surface and reaction rate.

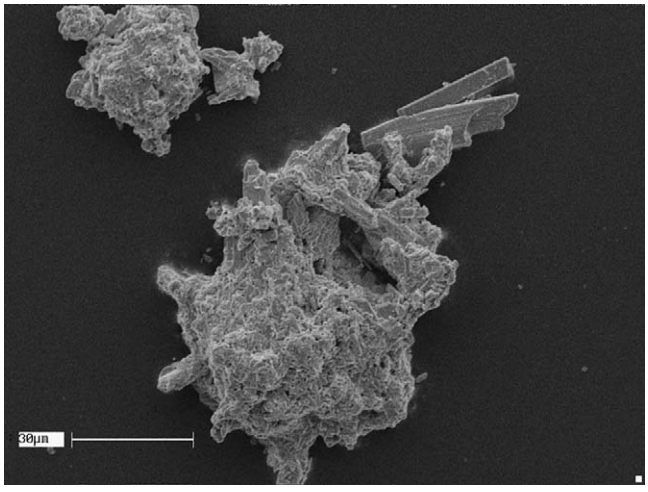

Fig. 11. SEM micrograph of TGA product at 350 °C (36 h milled molybdenite).

4. Conclusion

Mechanical activation of molybdenite causes the decrease in intensity of diffraction lines, the shift in diffraction lines and the diffraction line broadening. Mechanical activation decreases the ignition temperature of reaction from 470 to 180 °C after 36 h milling. The model-fitting kinetic approach of TGA data showed that the reaction mechanism for non-activated molybdenite is chemical control with $E = 34.25\,\text{kcal mol}^{-1}$ and $A = 2 \times 10^{8}\,\text{s}^{-1}$. In the activated molybdenite the reaction mechanism changed to diffusion control with $E = 60.55\,\text{kcal mol}^{-1}$ and $A = 6 \times 10^{19}\,\text{s}^{-1}$.

References

[1] P. Balaz, Extractive Metallurgy of Activated Minerals, Elsevier, Amsterdam, 2000.
[2] D. Tromans, J.A. Meech, Miner. Eng. 14 (11) (2001) 1359–1377.
[3] P.G. Fox, J. Mater. Sci. 10 (1975) 340–360.
[4] I.J. Lin, S. Nadiv, J. Mater. Sci. Eng. 39 (1979) 193–209.
[5] P.Yu. Butyagin, Colloid J. Russian Acad. Sci.: Kolloidnyi Zhurnal 61 (5) (1999) 537–544.
[6] H. Hu, Q. Chen, Z. Yin, G. Gottstein, et al., Metall. Mater. Trans.: B 35B (2004) 1203–1208.
[7] C.K. Gupta, Extractive Metallurgy of Molybdenum, CRC Press, USA, 1992.
[8] G.A. Mirson, A.N. Zelikman, Metallurgy of Rare Metals, Metallurgia Publ., Moscow, 1965.
[9] A.K. Galwey, M.E. Brown, Thermal Decomposition of Ionic Solids: Chemical Properties and Reactivities of Ionic Crystalline Phases, 2nd ed., Elsevier, Amsterdam, 1999, p. 75.
[10] A.M. Abdel-Rehim, J. Therm. Anal. Calorim. 57 (1999) 415.
[11] H. Polli, L.A.M. Pontes, A.S. Araujo, J. Therm. Anal. Calorim. 79 (2005) 383.
[12] A. Khawam, D.R. Flangan, Thermochim. Acta 436 (1/2) (2005) 101–112.
[13] S. Vyazovkin, C.A. Wight, Thermochim. Acta 340/341 (1999) 53.

[14] A. Mackovciacova, P. Balaz, Proceedings of the International Scientific Technical Seminar on Mechanochemistry and Mechanoactivation, St. Petersburg, 1995, pp. 110–114.
[15] S. Vyazovkin, C.A. Wight, Int. Rev. Phys. Chem. 117 (3) (1998) 407–433.
[16] T. Sun, Y. Zhao, J. Jin, D. Wang, J. Therm. Anal. 45 (1995) 1105.
[17] Z.H. Yang, X.Y. Li, Y.J. Wang, J. Therm. Anal. 48 (1997) 917.
[18] Q.P. Hu, X.G. Cui, Z.H. Yang, J. Therm. Anal. 48 (1997) 1379.
[19] P. Budrugeac, E. Segal, J. Therm. Anal. 49 (1997) 183.